LANGMUIR Article
Cite This: Langmuir 2019, 35, 14505−14510
pubs.acs.org/Langmuir

Effect of Electrolytes on Gas Oversolubility and Liquid Outflow from Hydrophobic Nanochannels

Lijiang Xu, Mingzhe Li, and Weiyi Lu*

Department of Civil and Environmental Engineering, Michigan State University, East Lansing, Michigan 48824, United States

Supporting Information

ABSTRACT: We have experimentally studied the effect of electrolytes on gas oversolubility and liquid outflow from hydrophobic nanochannels. By immersing nanoporous material with the same porous structure and surface properties into four different aqueous electrolyte solutions with the same surface tension, the excessive solid−liquid interfacial tension of the resulted liquid nanofoam (LN) systems has been set as a constant. Upon unloading, partial liquid outflow has been observed and quantified. As the four LN systems show different degrees of recoverability, it suggests that the degree of liquid outflow is highly sensitive to the ion species. In addition, different from bulk phase scenario, the anions have a more profound effect than cations on gas oversolubility. Lower bulk gas solubility and larger gas oversolubility factor lead to higher degree of liquid outflow and recoverability of the LN systems. This fundamental understanding on the mechanism of liquid outflow enables the development of nanofluidics-based system into reusable energy absorbers.

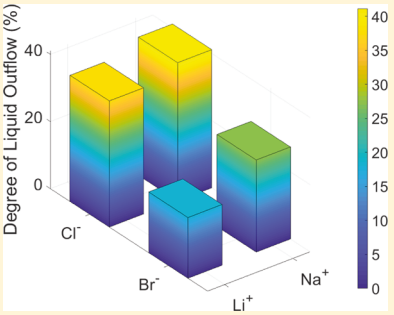

1. INTRODUCTION

Liquid motion in nanoenvironment has immense importance in various applications including gas and petroleum extraction and storage,[1,2] membrane-based osmosis and filtering process,[3,4] heterogeneous catalytic reactions,[5,6] and chromatographic analysis.[7] Recently, a unique force-aided liquid motion in hydrophobic nanochannels has been employed as a novel energy mitigation mechanism in a liquid nanofoam (LN) system.[8−10] In the LN system, particles containing open hydrophobic nanochannels are immersed in a nonwettable liquid. At ambient condition, the nanochannels are not accessible to the liquid molecules due to the surface energy barrier at the nanochannel entrance.[11] When an external pressure is applied and overcomes the surface energy barrier, the liquid molecules can be forced into and fill the hydrophobic nanochannels. Under quasi-static loading condition, large amount of mechanical energy is converted into solid−liquid interfacial energy and dissipated as heat during the filling. As the external applied pressure is released, the intruded liquid may partially or even fully flow out of the hydrophobic nanochannels. As the energy dissipation mechanism of the LN system is based on the force-aided nanoscale liquid motion rather than permanent crushing or plastic buckling of the nanochannels,[10] the LN system holds great promise for the development of reusable energy absorbers, which is particularly important for repetitive head impacts in sports and battlefield. The reusability of LN is determined by the degree of liquid outflow from the hydrophobic nanochannels when the external pressure is removed.

Previous studies have suggested that the degree of liquid outflow is related to the structure and morphology of the nanoporous network,[12−14] the excessive solid−liquid interfacial tension,[15,16] and the gas oversolubility in nanoenvironment.[17−19] However, there is lack of experimental validation for numerical models. For example, it was predicted by a molecular dynamic model that liquid outflow is impossible in nanochannels with pore size larger than 6 nm,[13] which is not true, as we have observed a partial liquid outflow in nanochannels with pore sizes of 120 nm in our previous studies[8,9] and 8.0 nm in this study. The challenge in understanding the liquid outflow mechanism by experimental approaches lies in the coupling effect of the above system determinants. Specifically, changes in the nanoporous network, such as the size, effective length, and surface condition of the nanochannels, vary the excessive solid−liquid interfacial tension suggested by the Young−Laplace equation[20] as well as the gas oversolubility.[14] Other experimental work based on a single nanoporous media[15,16] shed light on the effect of ion effect on the liquid outflow. However, the ion concentration in the electrolyte solutions has influence on both excessive solid−liquid interfacial tension and the gas oversolubility.

In this study, we have successfully decoupled the effect of gas oversolubility from the one of excessive solid−liquid interfacial tension by precisely adjusting the concentration of different electrolytes to keep the surface tension of all liquid phases the same. By immersing nanoporous material with same porous structure and surface properties into these aqueous electrolyte solutions, the excessive solid−liquid interfacial tension of the resulted LN systems has been set as a constant. This approach is capable of individually investigating the effect

Received: September 11, 2019
Revised: October 19, 2019
Published: October 22, 2019

DOI: 10.1021/acs.langmuir.9b02867
Langmuir 2019, 35, 14505−14510

of the gas oversolubility on the liquid outflow from hydrophobic nanochannels.

2. MATERIALS AND EXPERIMENT SETUP

The nanoporous material used in the current study was a surface-modified nanoporous silica gel (Fluka 100 C_8, Sigma Aldrich). The as-received material was in powder form, and the particle size was in the range of 40−63 μm. The naturally hydrophilic siliceous surface had been covered with alkyl chains and converted into a hydrophobic surface. The nanoporous structure of the material was characterized by a Brunauer−Emmett−Teller (BET) analyzer (ASAP 2020, Micromeritics). The measured specific surface area, average pore size, and pore volume of the nanoporous material were 227 m^2/g, 8.0 nm, and 0.43 cm^3/g, respectively.

Four types of aqueous electrolyte solutions with the same surface tension were prepared at 23 °C based on the linear relationship between molar concentrations of electrolytes and surface tension of the resulted aqueous solutions.[21−23] The corresponding molar concentrations of the electrolytes used in this study were 3.04 M NaCl, 3.37 M LiCl, 3.43 M NaBr, and 3.84 M LiBr. The detailed electrolyte molar concentration selection is described in the Supporting Information.

To prepare the LN specimens, 0.2 g of the hydrophobic silica gel was first placed at the bottom of a 316 stainless steel cell as depicted in Figure 1. Then, 2.3 mL of aqueous electrolyte solution was slowly dropped into the cell by glass Pasteur pipette. Once the cell was filled by the LN samples, it was sealed by an O-ring fixed on a 316 stainless steel piston. The diameter of the piston, d, was 12.7 mm. For each aqueous electrolyte solution, three LN specimens with the same particle and liquid contents were prepared and characterized by pressure-driven liquid infiltration tests.

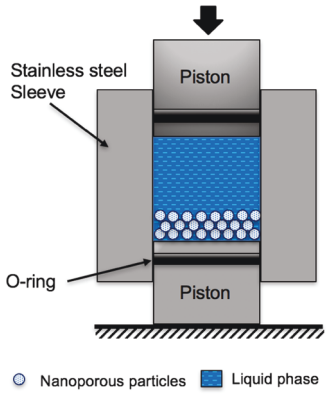

Figure 1. Schematic of LN specimen sealed in a testing cell with two pistons.

The sealed testing cell was placed on the platen of a universal tester (model 5982, Instron) and compressed at the speed of 2 mm/min. As an external force, F, was applied on the cell, a hydrostatic pressure, P, was built in the testing cell and applied on the sealed LN specimen. When the applied load reached 8 kN (equivalent to 63 MPa), the load cell of the Instron machine was moved back at the same speed. The externally applied hydrostatic pressure was calculated as $P = 4F/\pi d^2$. The specific volume change of the LN was calculated as $V = \Delta \cdot \pi d^2/4m$, where Δ and m were the measured displacement of the piston and the mass of the nanoporous silica gel, respectively. The loading−unloading cycles were repeated for 3 times for each LN specimen.

3. RESULTS AND DISCUSSION

Figure 2a shows the typical first loading−unloading cycles of LN specimens containing different aqueous electrolyte solutions. During the loading process, the initial response of all LN specimens is linearly elastic, as the externally applied hydrostatic pressure is not high enough to overcome the surface energy barrier between the hydrophobic nanopore surface and the nonwetting aqueous electrolyte solutions. As the pressure increases to the liquid infiltration pressure ($P_{in} \sim$ 17 MPa), the pressure of the first turning point of the loading curve, the liquid molecules are forced into and fill the nanochannels. The force-aided liquid filling process and the resulted pressure plateau are referred to as liquid infiltration and the liquid infiltration plateau, respectively. The relationship between the excessive solid−liquid interfacial tension, $\Delta\gamma$, and P_{in} can be described by the classic Laplace−Young equation as $P_{in} = 4\Delta\gamma/d_n$, where d_n is the nanopore diameter. Upon the completion of nanochannel filling, the slope of the loading curves quickly increases to a value that is slightly higher than the initial elastic one. As the nanochannels are filled with liquid, the nanoporous silica gel is turned into its solid counterpart, which has larger Young's and bulk moduli.

All the LN specimens have the same excessive solid−liquid surface tension, as they possess same P_{in} and the liquid infiltration plateau. The same excessive solid−liquid surface tension is also confirmed by the same surface tension of all four aqueous electrolyte solutions, ~77 mN/m, measured by a tensiometer (model 250, Ramé-Hart). Combining with the same porous structure and surface condition of the nanochannels, all the LN specimens have the same excessive solid−liquid surface tension. This is essential to study the gas phase effect on the liquid outflow as the same excessive solid−liquid surface tension ensures that the liquid outflow is initiated at the same condition.

During unloading, the internal pressure of the LN specimens drops linearly with a small volume change at the beginning.

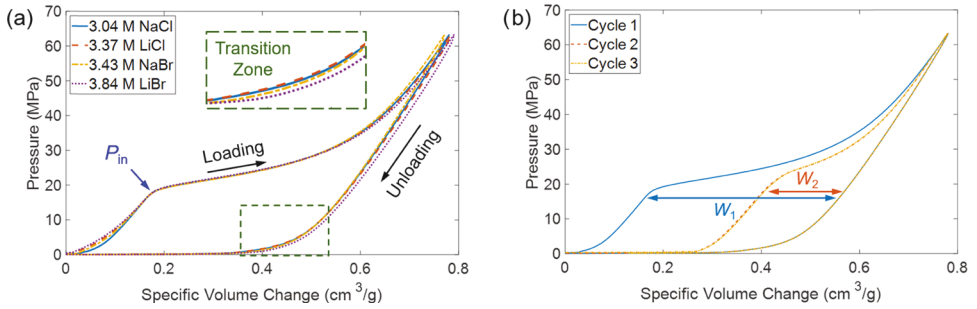

Figure 2. Typical loading−unloading cycles of LN specimens containing different aqueous electrolyte solutions: (a) typical first loading−unloading cycles of different LN specimens. The inset shows the difference in the transition zone of LN specimens containing different electrolytes and (b) the first three consecutive loading−unloading cycles of LN specimen with 3.04 M NaCl solution.

DOI: 10.1021/acs.langmuir.9b02867
Langmuir 2019, 35, 14505−14510

With further reduction in the internal pressure, a transition zone with a reduced slope is observed. The much reduced slope of the unloading curve as well as the associated large specific system volume change suggest that the confined liquid and gas molecules in the hydrophobic nanochannels start to flow out. The variation of the pressure associated with the transition zone (inset in Figure 2a) indicates the influence of the electrolyte types on the liquid outflow behavior.

Although the liquid outflow cannot be directly observed in the unloading portion of the first cycle due to the outflow of mixed liquid and gas from the nanochannel, the degree of liquid outflow can be determined by the liquid infiltration plateau of the second cycle. Figure 2b shows the first three consecutive loading–unloading curves of the LN specimen containing 3.04 M NaCl aqueous solution. By comparing the first two loading–unloading cycles, P_{in} is increased, while the width of the infiltration plateau is much reduced in the 2nd cycle. This indicates that only partial nanochannel volume is available for the liquid infiltration in the 2nd cycle, which is the volume of the liquid flowing out of the nanochannel during the unloading process of the 1st cycle. The width of infiltration plateau of each cycle is defined as the specific volume change between the loading and unloading curves at the pressure of 17 MPa, as illustrated in Figure 2b. As both the loading and unloading curves of 2nd and 3rd cycles of the LN specimen are nearly identical, only the width of the infiltration plateau of the 1st and 2nd cycles, W_1 and W_2, are measured and summarized in Table 1.

Table 1. Measured Infiltration Plateau Width and Degree of Liquid Outflow of LN Specimens

electrolyte solution	W_1 (mm^3/g)	W_2 (mm^3/g)	D_{out} (%)
3.04 M NaCl	395 ± 1	162 ± 4	41.2 ± 1.0
3.37 M LiCl	401 ± 10	151 ± 6	37.6 ± 0.7
3.43 M NaBr	395 ± 1	108 ± 10	27.4 ± 2.5
3.84 M LiBr	400 ± 3	72 ± 14	18.1 ± 3.3

The measured W_1 is close but smaller than the total pore volume of the nanoporous silica gel, which is due to the van der Waals distance between the liquid molecules and the hydrophobic wall of nanochannels.[24,25] The degree of liquid outflow equals the reusability of the LN specimens and is defined as $D_{out} = W_2/W_1$. For LN specimens containing other aqueous electrolyte solutions, the consecutive loading–unloading cycles have the same trend as the NaCl-based system presented in Figure 2b. All the typical loading–unloading cycles of LN specimens can be found in the Supporting Information (Figure S1). The calculated average degree of liquid outflow of LN specimens is plotted in Figure 3. Although all the LN systems have the same excessive solid–liquid interfacial tension, they have different degree of liquid outflow.

As all the LN specimens have the same liquid infiltration behavior, the ion effect on the liquid–solid interaction in the nanochannels is identical.[26−28] The variation in the degree of liquid outflow should be attributed to the ion effect on the liquid–gas interaction in the nanochannels. It has been found that the presence of electrolytes reduces the gas solubility in bulk phase due to the "salting-out" effect.[29−31] Following the model developed by Schumpe,[32] the bulk solubility of gas in the selected aqueous electrolyte solutions at ambient condition (1 atm, 23 °C), C_0, is calculated and shown in Table 2. The

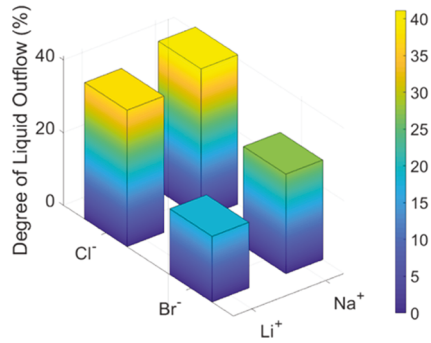

Figure 3. Ion effect on the degree of liquid outflow from hydrophobic nanochannels.

calculation method as well as the bulk gas solubility in pure water are detailed in the Supporting Information S3.

By following the slope of the unloading curve (dP/dV), the unloading process of LN specimens can be divided into three zones (Figure 4a). The first zone (Z_1, from point A to point B) is the linear expansion of the LN system that resulted from the reduced external pressure. The second zone (Z_2, from point B to point E) is defined as the transition zone of the liquid outflow. In the transition zone, the significantly dropped slope of the unloading curve indicates that with the same dP there is increased specific system volume recovery of the LN system. The pressure at point B of all LN systems (>18 MPa) significantly promotes bulk gas solubility. According to Henry's law, the bulk gas solubility is linearly proportional to the total pressure applied to the solution. The estimated bulk gas solubility and the internal pressure of the LN at point B are summarized in Table 2. Please note that even all the gas initially stored in the nanochannels (~3.29×10^{-6} mol) flows into the bulk liquid phase at this pressure, the gas can be fully dissolved by the bulk electrolyte solutions and would not have much effect on the system volume recovery. Therefore, the increased system volume recovery is due to the liquid outflow from the hydrophobic nanochannels. It is noticed that a higher P_B promotes the degree of liquid outflow of LN systems. The third zone (Z_3, from point E to point F) has the system volume recovery at a nearly constant internal pressure of the LN. The point F is the ending point of the unloading curve, where the crosshead of the Instron machine is detached from the testing cell and the internal pressure drops to 0 MPa. The total system volume recovery from point B to point F for all the LN specimens is close to the value of W_1. As only the partial space in the nanochannels is available for liquid infiltration in the 2nd loading, the total system volume recovery during the 1st unloading process is the combination of liquid and gas outflow from the nanochannels. Different from the loading process, the unloading portion of all 3 cycles follows the exact same path (Figure 2b). In each cycle, the nanochannels are fully filled by liquid and gas molecules at the peak loading pressure (point A). As the loading–unloading process is continuous, the gas diffusion, a slow time-dependent behavior, can be ignored. Therefore, the unloading process is reset to the same starting point at point A in every cycle.

As the crosshead of the Instron machine moves back at a constant speed, the specific volume change, dV, is proportional to time, dt. Therefore, the slope of the unloading curve is an analogue of the pressure drop speed in the nanochannels (dP/dt). Similarly, d^2P/dV^2 is an analogue of the pressure deceleration (d^2P/dt^2). By following the "pressure deceler-

DOI: 10.1021/acs.langmuir.9b02867
Langmuir 2019, 35, 14505−14510

Table 2. Estimated Bulk Phase Gas Solubility in Selected Aqueous Electrolyte Solutions at 23 °C

electrolyte solution	C_0 (M)	P_B (MPa)	C_B (M)	P_E (MPa)	C_E (M)	f	C_{Nano} (M)
3.04 M NaCl	2.85×10^{-4}	27.7 ± 1.4	7.85×10^{-2}	0.45 ± 0.10	1.55×10^{-3}	27.0	7.70×10^{-3}
3.37 M LiCl	3.71×10^{-4}	26.7 ± 0.5	9.83×10^{-2}	0.51 ± 0.02	2.23×10^{-3}	18.5	6.85×10^{-3}
3.43 M NaBr	2.92×10^{-4}	25.8 ± 1.8	7.49×10^{-2}	0.65 ± 0.13	2.18×10^{-3}	19.3	5.63×10^{-3}
3.84 M LiBr	3.97×10^{-4}	18.9 ± 2.4	7.46×10^{-2}	0.68 ± 0.10	3.08×10^{-3}	13.5	5.36×10^{-3}

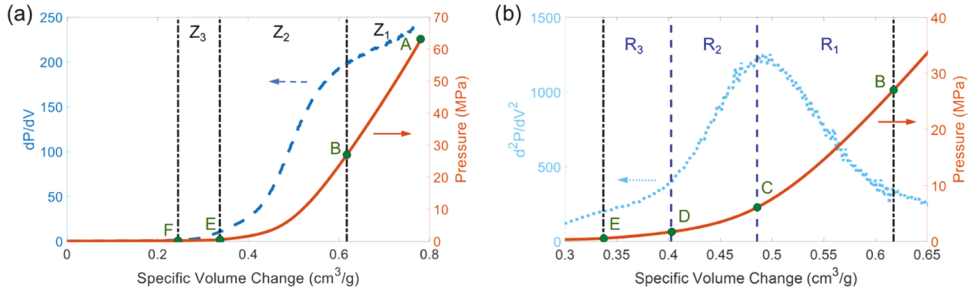

Figure 4. Unloading process of the LN system based on the NaCl solution. (a) Linear expansion, transition, and stabilized zones of the unloading curve. (b) Subdivided regions of the transition zone, Z_2.

ation", the transition zone can be subdivided into 3 regions (Figure 4b). In the 1st region (R_1, from point B to point C), the "pressure deceleration" increases. As the pressure in the nanochannels is proportional to the spacing between liquid molecules, i.e., the potential energy of liquid molecules, the increase in pressure deceleration indicates an accelerated mass transport from nanochannels to the bulk phase. As the weight of gas is negligible compared to that of liquid, R_1 is dominated by the liquid outflow. In addition, due to the oversolubility,[19,33] the liquid phase confined in nanochannels can uptake much more gas than the bulk liquid phase. The gas–liquid interaction is much stronger in the nanochannels than in the bulk phase. Therefore, most of the gas molecules are retained in the nanochannels. Accompanied with the liquid outflow, the gas concentration in the nanochannels increases, while the potential energy of the liquid molecules decreases quickly. At point C, the pressure deceleration reaches its maximum value and starts to decrease, indicating a reduced liquid outflow. In the 2nd region (R_2, from point C to point D), as the pressure drop speed still decreases, the increasing system volume recovery is mainly contributed by gas outflow. This is attributed to the increased gas concentration in the nanochannels. In the 3rd region (R_3, from point D to point E), the pressure deceleration starts to converge to a constant. This is because the gas escaping from the nanochannels is dissolved by the bulk liquid phase. With the reduced pressure and the increased gas content, the bulk liquid phase is saturated with gas and suppresses the gas outflow. The saturated bulk liquid phase is proven by the gas precipitation at further reduced pressure. Gas bubbles have been observed in our previous study.[14]

At point E, the pressure deceleration and the pressure in the nanochannels are nearly constants. At this low pressure level, the gas molecules may not be fully dissolved and the pressure change in the nanochannels is more sensitive to the gas volume change rather than the potential energy of the liquid molecules. To maintain the pressure inside the nanochannels, with one unit volume of liquid outflow, one unit volume of gas is precipitated out from the confined liquid molecules. Thus, at point E, the confined liquid in the nanochannels is also saturated with gas. The corresponding gas solubility is about 4.12×10^{-2} M (one unit volume of gas fully dissolved in one unit volume of liquid), which is much higher than the calculated C_E listed in Table 2. The ratio between the nano and bulk gas solubilities is the oversolubility factor, f. The values of f are summarized in Table 2. These experimental results are at the same order of values predicted by previous numerical results.[16] The smaller values are due to the presence of electrolytes.

The ion species have influence on C_0, f, and D_{out}. In the bulk phase, cation has more prominent effect on gas solubility, as Na^+-based systems have a much reduced gas solubility. This is due to the solvated cation structure in the solution. In the nanochannels, both cation and anion have significant effect on the oversolubility factor. This is because of the unique ion structure in the nanochannels, where the solvated cation structure cannot fully developed.[28] Instead, the anions have a stronger interaction with the water molecules that can otherwise dissolve gas molecules.[31] Na^+ has less effect on f than Li^+, as the f values in Na^+-based solutions are closer to that in pure water. Similarly, Cl^- has less effect on f than Br^-. Consequently, the pair of Na^+ and Cl^- has the least effect on f, while the pair of Li^+ and Br^- dramatically reduces f. For LiCl and NaBr solutions, their oversolubility factors are similar and in between the values of NaCl and LiBr.

The gas oversolubility in nanochannels of each electrolyte solution at ambient condition, C_{Nano}, can be calculated as $C_0 \cdot f$ and is listed in Table 2. It seems that a higher gas oversolubility leads to a higher degree of liquid outflow. However, when the C_{Nano} has a higher value, its effect on liquid outflow is weaker (Figure 5). In addition, D_{out} is more sensitive to the species of anion than that of cation as shown in Figure 3. This is different from the effect of electrolytes on f. The electrolyte solutions with a higher C_{Nano} have a stronger interaction with gas molecules and can accommodate more gas molecules in the nanochannels, and thus retain more gas in R_1.

In R_2, gas molecules start to escape from the nanochannels. The loss of gas content in the nanochannels equals to the reduced reusability of the system and can be seized only when the bulk liquid phase is saturated with gas. In our previous study,[14] D_{out} dramatically reduces when the liquid phase has been degassed before the infiltration test. The initial bulk gas concentration is lower than C_0 due to degassing. More gas outflow is required to saturate the bulk liquid phase and shut

DOI: 10.1021/acs.langmuir.9b02867
Langmuir 2019, 35, 14505−14510

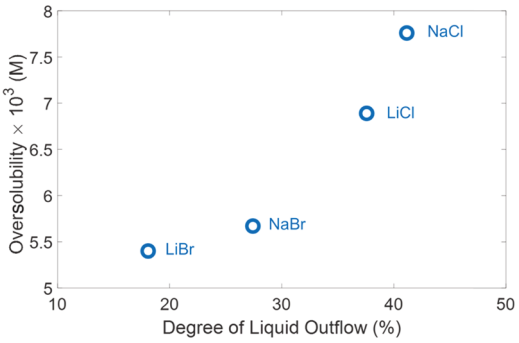

Figure 5. Effect of gas oversolubility on the degree of liquid outflow from the nanochannels.

down the gas outflow in R_2. Therefore, gas-saturated bulk liquid phase with lower C_0 is desired to quickly shut down the gas transportation from the nanochannels to the bulk phase and enhance D_{out}.

4. CONCLUSIONS

In summary, the effect of gas oversolubility on liquid outflow from hydrophobic nanochannels has been investigated independently by maintaining the same excessive solid−liquid interfacial tension. The pairs of cations and anions not only alter the gas solubility in bulk phase but also affect the gas oversolubility factor in nanochannels. The degree of liquid outflow from hydrophobic nanochannels is determined by both the bulk solubility and the oversolubility factor. Lower bulk gas solubility and larger gas oversolubility factor in nanochannels lead to a higher degree of liquid outflow and the reusability of LN system. In contrast to the bulk phase, anion has more effect on the degree of liquid outflow and the system reusability than cation. These findings not only provide design guidelines for reusable nanofluidics-based energy absorbers but also extend the knowledge of gas−liquid interaction in a confined environment.

■ ASSOCIATED CONTENT

Supporting Information

The Supporting Information is available free of charge on the ACS Publications website at DOI: 10.1021/acs.langmuir.9b02867.

Table S1: surface tension and air solubility of selected aqueous electrolyte solutions at 23 °C; Table S2: gas solubility in pure water at 23 °C; Table S3: ion-specific parameters and molar concentration at 23 °C; Figure S1: typical loading−unloading curves of LN systems containing different aqueous electrolyte solutions; the 2nd and 3rd cycles are almost identical for all LN systems (PDF)

■ AUTHOR INFORMATION

Corresponding Author

*E-mail: wylu@egr.msu.edu. Phone: (517) 353-6448.

ORCID

Weiyi Lu: 0000-0003-1069-3480

Notes

The authors declare no competing financial interest.

■ ACKNOWLEDGMENTS

The authors would like to thank Alex Mirabal and Dr. Scott Barton to provide help on the BET analysis on the nanoporous structure of the silica gel and Charifa Hejase and Dr. Volodymyr Tarabara to provide help on the measurement of the surface tension of the aqueous electrolyte solutions. This study is financially supported by NSF CBET-1803695.

■ REFERENCES

(1) Rallabandi, P. S.; Ford, D. M. Permeation of small molecules through polymers confined in mesoporous media. *J. Membr. Sci.* **2000**, *171*, 239−252.
(2) Guo, C.; Xu, J.; Wu, K.; Wei, M.; Liu, S. Study on gas flow through nano pores of shale gas reservoirs. *Fuel* **2015**, *143*, 107−117.
(3) Bhattacharyya, D.; Butterfield, D. A. *Membrane Contactors: Recent Developments. New Insights into Membrane Science and Technology: Polymeric and Biofunctional Membranes*; Elsevier, 2003; Vol. *8*, pp 147.
(4) Bazhenov, S. D.; Lyubimova, E. S. Gas−liquid membrane contactors for carbon dioxide capture from gaseous streams. *Pet. Chem.* **2016**, *56*, 889−914.
(5) Guo, Y.; Langley, K. H.; Karasz, F. E. Nonanomalous diffusion in Vycor porous glass. *Phys. Rev. B: Condens. Matter Mater. Phys.* **1994**, *50*, 3400−3403.
(6) Dupont, J.; Fonseca, G. S.; Umpierre, A. P.; Fichtner, P. F.; Teixeira, S. R. Transition-metal nanoparticles in imidazolium ionic liquids: recycable catalysts for biphasic hydrogenation reactions. *J. Am. Chem. Soc.* **2002**, *124*, 4228−4229.
(7) Wuhrer, M.; Koeleman, C. A.; Hokke, C. H.; Deelder, A. M. Protein glycosylation analyzed by normal-phase nano-liquid chromatography− mass spectrometry of glycopeptides. *Anal. Chem.* **2005**, *77*, 886−894.
(8) Li, M.; Lu, W. Liquid marble: A novel liquid nanofoam structure for energy absorption. *AIP Adv.* **2017**, *7*, No. 055312.
(9) Li, M.; Lu, W. Adaptive liquid flow behavior in 3D nanopores. *Phys. Chem. Chem. Phys.* **2017**, *19*, 17167−17172.
(10) Zhang, Y.; Li, M.; Gao, Y.; Xu, B.; Lu, W. Compressing liquid nanofoam systems: liquid infiltration or nanopore deformation? *Nanoscale* **2018**, *10*, 18444−18450.
(11) Hu, D.; Jiang, H.; Meng, K.; Xu, J.; Lu, W. The impact mitigation of a heterojunction nanotube−water system: behavior and mechanism. *Phys. Chem. Chem. Phys.* **2016**, *18*, 7395−7403.
(12) Qiao, Y.; Cao, G.; Chen, X. Effects of gas molecules on nanofluidic behaviors. *J. Am. Chem. Soc.* **2007**, *129*, 2355−2359.
(13) Lefevre, B.; Saugey, A.; Barrat, J. L.; Bocquet, L.; Charlaix, E.; Gobin, P. F.; Vigier, G. Intrusion and extrusion of water in hydrophobic mesopores. *J. Chem. Phys.* **2004**, *120*, 4927−4938.
(14) Li, M.; Xu, L.; Lu, W. Nanopore size effect on critical infiltration depth of liquid nanofoam as a reusable energy absorber. *J. Appl. Phys.* **2019**, *125*, No. 044303.
(15) Surani, F. B.; Qiao, Y. Infiltration and defiltration of an electrolyte solution in nanopores. *J. Appl. Phys.* **2006**, *100*, No. 034311.
(16) Lu, W.; Kim, T.; Punyamurtula, V. K.; Han, A.; Qiao, Y. Effects of addition of potassium chloride and ethylene glycol on nanofluidic behaviors. *J. Mater. Sci.* **2011**, *46*, 4053−4057.
(17) Luzar, A.; Bratko, D. Gas solubility in hydrophobic confinement. *J. Phys. Chem. B* **2005**, *109*, 22545−22552.
(18) Miachon, S.; Syakaev, V. V.; Rakhmatullin, A.; Pera-Titus, M.; Caldarelli, S.; Dalmon, J. A. Higher gas solubility in nanoliquids. *ChemPhysChem* **2008**, *9*, 78−82.
(19) Ho, L. N.; Schuurman, Y.; Farrusseng, D.; Coasne, B. Solubility of gases in water confined in nanoporous materials: ZSM-5, MCM-41, and MIL-100. *J. Phys. Chem. C* **2015**, *119*, 21547−21554.
(20) Young, T. III. An essay on the cohesion of fluids. *Philos. Trans. R. Soc. London* **1805**, *95*, 65−87.
(21) Weissenborn, P. K.; Pugh, R. J. Surface tension of aqueous solutions of electrolytes: relationship with ion hydration, oxygen

DOI: 10.1021/acs.langmuir.9b02867
Langmuir 2019, 35, 14505−14510

solubility, and bubble coalescence. *J. Colloid Interface Sci.* **1996**, *184*, 550−563.
(22) Boström, M.; Williams, D. R.; Ninham, B. W. Surface tension of electrolytes: specific ion effects explained by dispersion forces. *Langmuir* **2001**, *17*, 4475−4478.
(23) Weissenborn, P. K. Surface Tension of Aqueous Electrolytes. *Encyclopedia of Surface and Colloid Science*; CRC Press, 2015; pp 7111−7115.
(24) Xu, B.; Qiao, Y.; Zhou, Q.; Chen, X. Effect of electric field on liquid infiltration into hydrophobic nanopores. *Langmuir* **2011**, *27*, 6349−6357.
(25) Beckstein, O.; Sansom, M. S. Liquid−vapor oscillations of water in hydrophobic nanopores. *Proc. Natl. Acad. Sci. USA* **2003**, *100*, 7063−7068.
(26) Liu, L.; Chen, X.; Lu, W.; Han, A.; Qiao, Y. Infiltration of electrolytes in molecular-sized nanopores. *Phys. Rev. Lett.* **2009**, *102*, No. 184501.
(27) Kim, T.; Lu, W.; Han, A.; Punyamurtula, V. K.; Chen, X.; Qiao, Y. Effects of anion concentration on ion-transport pressure in nanopores. *Appl. Phys. Lett.* **2009**, *94*, No. 013105.
(28) Han, A.; Lu, W.; Kim, T.; Chen, X.; Qiao, Y. Influence of anions on liquid infiltration and defiltration in a zeolite Y. *Phys. Rev. E* **2008**, *78*, No. 031408.
(29) Clever, H. L.; Holland, C. J. Solubility of argon gas in aqueous alkali halide solutions. Temperature coefficient of the salting out parameter. *J. Chem. Eng. Data* **1968**, *13*, 411−414.
(30) Long, F. A.; McDevit, W. F. Activity coefficients of nonelectrolyte solutes in aqueous salt solutions. *Chem. Rev.* **1952**, *51*, 119−169.
(31) Ruetschi, P.; Amlie, R. F. Solubility of hydrogen in potassium hydroxide and sulfuric acid. Salting-out and hydration. *J. Phys. Chem. A.* **1966**, *70*, 718−723.
(32) Schumpe, A. The estimation of gas solubilities in salt solutions. *Chem. Eng. Sci.* **1993**, *48*, 153−158.
(33) Hu, Y.; Huang, L.; Zhao, S.; Liu, H.; Gubbins, K. E. Effect of confinement in nano-porous materials on the solubility of a supercritical gas. *Mol. Phys.* **2016**, *114*, 3294−3306.

DOI: 10.1021/acs.langmuir.9b02867
Langmuir 2019, 35, 14505−14510